A coupled-channel deperturbation treatment of the $X^2\Sigma^+ \sim A^2\Pi \sim B^2\Sigma^+$ complex of CN radical towards a spectroscopic accuracy

V. A. Terashkevich, E. A. Pazyuk, A. V. Stolyarov*

Department of Chemistry, Lomonosov Moscow State University, 119991, Moscow, Leninskie gory 1/3, Russia

S. N. Yurchenko

Department of Physics and Astronomy, University College London, Gower St, London WC1E 6BT, UK

Abstract

A global deperturbation analysis of the experimental rovibronic term values of the $X^2\Sigma^+$, $A^2\Pi$ and $B^2\Sigma^+$ states of the $^{12}C^{14}N$ isotopomer has been performed. An inverse spectroscopic problem was directly solved in the framework of the reduced 4×4 coupled-channel (CC) deperturbation model based on potential energy curves (PECs) as well as the spin-orbit and L-uncoupling electronic matrix elements between the $X^2\Sigma^+$, $A^2\Pi$ and $B^2\Sigma^+$ states. The regular perturbations of the $X \sim A \sim B$ complex by remote states manifold were also taken into accounted by the introduction of the fine-structure Λ-doubling parameters being explicit functions of interatomic distance. The optimized PECs and electronic coupling parameters represent a vast majority (5600-6570) of the empirical termvalues belonging to locally and regularly perturbed levels of the $X \sim A \sim B$ complex with r.m.s. deviation about 0.015-0.05 cm^{-1}, which becomes comparable with a spectroscopic accuracy. The resulting mass-invariant CC deperturbation parameters improve a line-list propagation into a wide region of vibrational and rotational quantum numbers for all CN isotopomers.

Keywords: CN radical, electronic states, deperturbation analysis, coupled-channel approximation

1. Introduction

The diatomic CN radical is known primarily as one of the first molecule to be discovered in the interstellar medium (ISM) [1], which causes a persistent interest in the field of astrophysics and astrochemistry to this object. At the moment, the astronomical application of the energy, radiative, collisional and magnetic properties of the gas-phase CN radical involves, but is not limited to the following issues: measurements of the temperature of the background radiation [2]; determination of the chemical composition and time evolution of comet comas [3, 4]; the modeling of stellar nucleosynthesis [3], including a carbon and nitrogen abundance and their isotopic ratios;

*Corresponding author. E-mail: avstol@phys.chem.msu.ru; tel.: +7-495-939-12-93

a radiative association and cooling during of the C and N atoms collision; a probe of possible variation of fundamental (dimensionless) physical constants in the cosmological time scale [5]. The relative intensity distribution in strong emission bands spectra of CN radical are widely used in non-contact (optical) temperature measurements of the flame and plasma. In particular, laser-induced breakdown spectroscopy (LIBS) often exploits in the "violet" ($B^2\Sigma^+ - X^2\Sigma^+$) band system of the CN radical for the carbon atom analysis in organic compounds in an air.

The permanent, long and successful history of the spectroscopic study of the CN radical in UV, IR and MW regions has led to the accumulation of a huge (but not comprehensive) line-list of experimental rovibronic transitions, the overwhelming majority of which is related to the lowest three $X^2\Sigma^+$, $A^2\Pi$ and $B^2\Sigma^+$ electronic states (see Fig. 1). The measured active rotational-vibrational energy levels (MARVEL) approach [6] has been recently [7] applied for the statistically justified transformation of the measured lines positions to the corresponding rovibronic term values. The spectroscopic model independent MARVEL procedure provided about 6860 empirical term values covering the $v_X \in [0, 18]$, $v_A \in [0, 22]$ and $v_B \in [0, 19]$ vibrational levels of the $X^2\Sigma^+ \sim A^2\Pi \sim B^2\Sigma^+$ complex for the most naturally abundant $^{12}C^{14}N$ isotopomer.

All vibrational levels belonging to the $X \sim A \sim B$ complex (including the lowest terms of the ground state) undergo a *regular* rotational e/f-parity perturbations caused by a combination of the spin-orbit (SO) and L-uncoupling intramolecular interactions with the remote doublet and quartet states manifold. These normally weak perturbations appear in the observed spectra as so-called Λ-doubling effect [8] which monotonically increases as a rotational excitation increases. Furthermore, some excited rovibronic levels of the $X \sim A \sim B$ complex undergo the strong *local* perturbations caused by the mutual spin-orbit and electronic-rotational interactions between close-lying (accidentally almost degenerate) levels of the complex. The most pronounced *local* perturbations are taking place in the $B^2\Sigma^+$ state as this excited state additionally interacts with the nearby "dark" quartet states manifold (Fig. 1).

These local perturbations were partly deperturbed exploiting the band-by-band version of the traditional Effective Hamiltonian approach (EHA) [9]. Regular perturbed levels of the $X \sim A \sim B$ complex were also successfully treated in the framework of the conventional EHA providing the description of the measured line positions with almost experimental accuracy. The resulting deperturbed structure parameters of the $X^2\Sigma^+$, $A^2\Pi$ and $B^2\Sigma^+$ states were then combined with the *ab initio* evaluated $B - X$, $B - A$ and $A - X$ transition dipole moments [10] to generate a Molecular Line Lists, Intensities and Spectra (MoLLIST) data set for the $X \sim A \sim B$ complex [11] by means of LEVEL [12] and PGOPHER programs [13].

Unfortunately, the conventional EHA normally does't reproduce both *local* and *regular* perturbations observed in a wide energy excitation range on the same experimental level of accuracy. The EHA can interpolates missing lines with almost required spectroscopic accuracy, but can not predict spectra very well outside a experimental region because of principal limitations of perturbation theory. An alternative coupled-channel (CC) spectroscopic model, in principle, allows one to describe all perturbations on the same level of accuracy. The inverted CC method based on the DUO paradigm [14] has been recently used to accomplish a global deperturbation analysis of the $X \sim A \sim B$ complex of CN [15]. However, the resulting molecular parameters of the reduced 4×4 CC model (including potential energy curves of the coupled states, non-adiabatic spin-orbit and L-uncoupling matrix elements as a function of r) could reproduce overall set of the experimental term values of the $X \sim A \sim B$ complex with r.m.s. deviation of about 0.05-1.0 cm^{-1}, that is more than order higher the accuracy of spectroscopic measurements.

At the present work, overall accuracy of the CC deperturbation model has been significantly improved by taking into account for numerous regular interactions of the remote states manifold

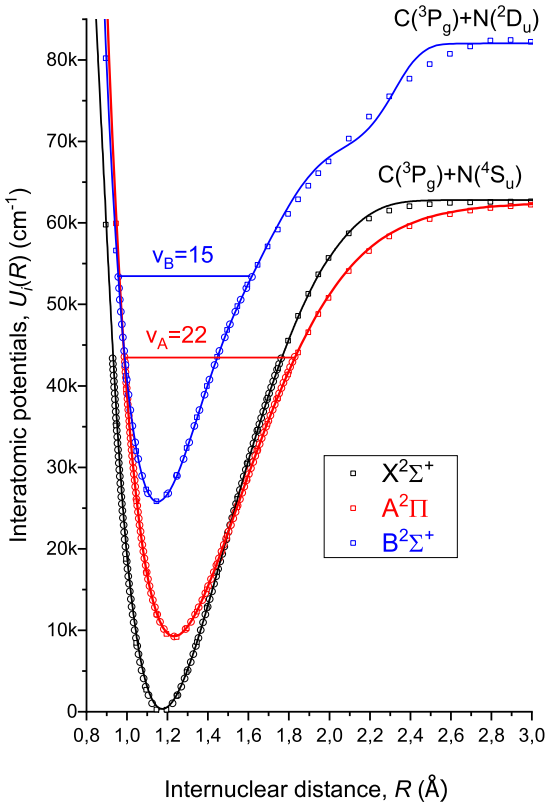

Figure 1: The empirical and *ab initio* potential energy curves for $X^2\Sigma^+$, $A^2\Pi$ and $B^2\Sigma^+$ states of CN radical. Solid lines are the empirical EMO potentials obtained in present work using the `set-II` of the Marvel experimental term values [6] (see Table 1 for details). Open squares are the *ab initio* potentials borrowed from Ref. [16]. Open circles are the experimental Rydberg-Klein-Rees (RKR) potentials constructed using the molecular constants from Refs. [17, 11].

with the $X^2\Sigma^+ \sim A^2\Pi \sim B^2\Sigma^+$ complex. It has been particularly realized by introducing in the reduced 4×4 CC Hamiltonian the mass-invariant Λ-doubling parameters being explicit functions of interatomic distance r.

2. Deperturbation Machinery

2.1. Modeling Hamiltonian

The rovibronic non-adiabatic energy $E^{e/f}$ (eigenvalues) and corresponding multi-component vibrational wave function $\mathbf{\Phi}$ (eigenfunctions) were determined (neglecting a hyperfine structure of the doublet states) for both e and f parity levels of the $X^2\Sigma^+ \sim A^2\Pi \sim B^2\Sigma^+$ complex of CN radical by solving four coupled-channel (CC) equations [14]:

$$\left(-\mathbf{I}\frac{\hbar^2 d^2}{2\mu dr^2} + \mathbf{V}^{e/f}(r;\mu,J) - \mathbf{I}E^{e/f}\right)\mathbf{\Phi}(r) = 0, \qquad (1)$$

with the conventional boundary $\phi_i(0) = \phi_i(\infty) = 0$ and normalization $\sum_i P_i = 1$ conditions, where $P_i = \langle\phi_i|\phi_i\rangle$ is the fractional partition of the $X \sim A \sim B$ level and $i \in [X^2\Sigma^+, A^2\Pi_{1/2}, A^2\Pi_{3/2}, B^2\Sigma^+]$. $\mathbf{I}$ is the identity matrix, μ is the reduced molecular mass, J is the rotational quantum number, $\mathbf{V}^{e/f}(r;\mu,J)$ - is the r-depending 4×4 matrix of potential energy.

The diagonal matrix elements of $\mathbf{V}^{e/f}(r;\mu,J)$ were specified in the form:

$$\begin{aligned} V^{e/f}_{X-X} = U_X &+ B\left[Y(Y\mp 1) + \gamma_X(1\mp Y)\right] \\ &+ B^2\left[q_X(1\mp Y)^2\right] \end{aligned} \tag{2}$$

$$\begin{aligned} V^{e/f}_{A_{3/2}-A_{3/2}} = U_A + A^{so} &+ B\left[Y^2-2\right] \\ &+ B^2\left[q_A(Y^2-1) + q_{A\Delta}(Y^2-4)\right] \end{aligned} \tag{3}$$

$$\begin{aligned} V^{e/f}_{A_{1/2}-A_{1/2}} = U_A - A^{so} &+ B\left[Y^2 + p_A(1\mp Y)\right] \\ &+ B^2\left[q_A(1\mp Y)^2 + q_{A\Delta}(Y^2-1)\right] \end{aligned} \tag{4}$$

$$V^{e/f}_{B-B} = U_B + B\left[Y(Y\mp 1)\right] \tag{5}$$

where we have used the notation

$$Y \equiv J + 1/2; \qquad B \equiv \frac{\hbar^2}{2\mu r^2},$$

and a sign $\mp$ refers to energy levels e- and f-parity, respectively.

The non-vanishing off-diagonal matrix elements of the $\mathbf{V}^{e/f}(r;\mu,J)$ were defined as

$$V^{e/f}_{A_{1/2}-A_{3/2}} = -B\left[1 + \frac{p_A + p_{A\Delta}}{2} + Bq_A(1\mp Y)\right]\sqrt{Y^2-1} \tag{6}$$

$$V^{e/f}_{A_{1/2}-X} = V^{so}_{AX} + BL_{AX}(1\mp Y); \quad V^{e/f}_{A_{3/2}-X} = -BL_{AX}\sqrt{Y^2-1} \tag{7}$$

$$V^{e/f}_{A_{1/2}-B} = V^{so}_{AB} + BL_{AB}(1\mp Y); \quad V^{e/f}_{A_{3/2}-B} = -BL_{AB}\sqrt{Y^2-1} \tag{8}$$

All electronic parameters in the CC deperturbation model are tacitly assumed to be explicit functions of interatomic distance r. In particular, $U_i(r)$ are the conventional potential energy curves (PECs) of the isolated $i \in [X^2\Sigma^+, A^2\Pi, B^2\Sigma^+]$ states corresponding to the pure Hund's case "**a**". The $A^{so}(r)$ is the spin-orbit splitting function of the $A^2\Pi$ state. $V^{so}_{AB}(r)$ and $V^{so}_{AX}(r)$ are electronic spin-orbit coupling matrix elements between the $A^2\Pi$ and $X, B^2\Sigma^+$ states whereas $L_{AB}(r)$, $L_{AX}(r)$ are the L-uncoupling (Coriolis) non-adiabatic matrix elements.

A key characteristic of the present CC treatment of the $X \sim A \sim B$ complex is accounted for regular interactions of the complex by remote doublet states manifold in the framework of the 2-nd order Van-Vleck contact transformation [18]. It has been done by the introduction in the reduced coupled-channel (RCC) model [19], the so-called fine-structure Λ-doubling parameters being mass-independent functions of r [8]. For instance, the $\gamma_X(r)$ and $q_X(r)$ functions [20] in

Eq.(2) are responsible for spin-orbit and L-uncoupling interactions of the ground X-state with the $^2\Pi$ states, skipping the $A^2\Pi$ state. The $p_A(r)$ and $q_A(r)$ functions involved in Eqs.(3), (4) and (6) take into account for an intramolecular interaction of the $A^2\Pi$ state with the $^2\Sigma^{\pm}$ states manifold, excluding the lowest $(X, B)^2\Sigma^+$ members. The $p_{A\Delta}(r)$ and $q_{A\Delta}(r)$ functions are arisen from interaction of the $A^2\Pi$ state with the higher-lying $^2\Delta$ states. At the same time, the deperturbation model above has completely ignored an influence of the quartet states manifold.

It should be noticed that the required spin-orbit and L-uncoupling electronic matrix elements between the low-lying doublet states of CN became recently available from the relevant electronic structure calculations [16]. These *ab initio* calculations have demonstrated the surprisingly small contribution of the higher-lying $^2\Pi$ states manifold into the γ and q parameters of the excited $B^2\Sigma^+$ state comparing with their impact to the ground $X^2\Sigma^+$ state. This is the reason why the corresponding Λ-doubling parameters of the B-state were neglected in the modeling Hamiltonian above (see Eq.(5)).

2.2. Approximation of electronic parameters

The interatomic PECs $U_i(r)$ for all three states of the $X \sim A \sim B$ complex were approximated by the analytical Extended Morse Oscillator (EMO) form [21, 22]:

$$U_i^{EMO}(r) = T_{\rm e} + D_{\rm e}\left[1 - e^{-\beta(r)(r-r_{\rm e})}\right]^2 \tag{9}$$

where $T_{\rm e}$ is the electronic term, $D_{\rm e}$ is the dissociation energy and $r_{\rm e}$ is the equilibrium distance. In contrast to the conventional Morse potential, the r-depending exponent coefficient $\beta(r)$ in Eq.(9) is defined as the polynomial series

$$\beta(r) = \sum_{i=0}^{N} \beta_i [y_p(r)]^i \tag{10}$$

with respect to the reduced coordinate [23]

$$y_p(r) = \frac{r^p - r_{\rm ref}^p}{r^p + r_{\rm ref}^p}; \quad y_p \in [-1; 1] \tag{11}$$

where p is the integer number and $r_{\rm ref}$ is the reference distance.

Both on-diagonal (3-4) and off-diagonal (6-8) spin-orbit and L-uncoupling electronic matrix elements between the $X^2\Sigma^+$, $A^2\Pi$ and $B^2\Sigma^+$ states were constructed as *morphed* functions of their *ab initio* counterparts $f^{ab}(r)$ [16]:

$$f^{morph}(r) = S(r)[f^{ab}(r) - f_\infty] + f_\infty \tag{12}$$

where the f_∞ is the asymptotic value of the corresponding matrix element on a dissociation (atomic) limit. The *ab initio* point-wise $f^{ab}(r_i)$ matrix elements were interpolated by ordinary cubic splines with so-called "natural" boundary conditions to construct continua $f^{morph}(r)$ functions.

The so-scaled "scaling" function $S(r)$ in Eq.(12), was defined to be a linear function of the reduced coordinate $y_{p=1}$ (see Eq.(11)):

$$S(r) = \alpha_0 + \alpha_1 y_{p=1} \tag{13}$$

where the expansion coefficients α_i are adjusted parameters with the initial values $\alpha_0 = 1$ and $\alpha_1 = 0$, respectively.

The Λ-doubling functions belonging to the $A^2\Pi$ state $p_A(r)$, $q_A(r)$, $p_{A\Delta}(r)$ and $q_{A\Delta}(r)$ were approximated by the linear function (13) as well. The corresponding radial functions of the ground X-state $\gamma_X(r)$ and $q_X(r)$ in Eq.(2) were determined as

$$\gamma_X(r) = S(r)\left[\sum_{j\in^2\Pi}\frac{2V^{so}_{Xj}L_{Xj}}{\Delta U_{Xj}}\right]; \quad q_X(r) = \sum_{j\in^2\Pi}\frac{|L_{Xj}|^2}{\Delta U_{Xj}} \tag{14}$$

where $\Delta U_{Xj}(r) = U_X(r) - U_j(r)$ and $j \neq A^2\Pi$. The required *ab initio* spin-orbit $V^{so}_{Xj}(r)$ and L-uncoupling $L_{Xj}(r)$ electronic matrix elements (along with the relevant adiabatic PECs for the ground and excited $^2\Pi$ states) were borrowed from Ref. [16].

2.3. Fitting procedure

The trial set of electronic parameters included in the reduced 4×4 matrix of potential energy $\mathbf{V}^{e/f}(r;\mu,J)$ of the CC Hamiltonian (1) has been iteratively refined during the Levenberg-Marquard minimization of the sum of squares: $\chi^2_{total}(\mathrm{a_p}) = \chi^2_{exp} + \chi^2_{ab}$, where the first term is

$$\chi^2_{exp} = \sum_{j=1}^{N^{exp}_{fit}}\left(\frac{E^{exp}_j + ZPE_{fit} - E^{CC}_j}{\sigma^{exp}_j}\right)^2 \tag{15}$$

while the second one:

$$\begin{aligned}\chi^2_{ab} = &\sum_i\sum_{k=1}^{N^{ab}}\left(\frac{U^{EMO}_i(r_k) - U^{ab}_i(r_k)}{\sigma^{ab}_i(r_k)}\right)^2 \\ &+ \sum_j\sum_{k=1}^{N^{ab}}\left(\frac{f^{morph}_j(r_k) - f^{ab}_j(r_k)}{\sigma^{ab}_j(r_k)}\right)^2\end{aligned} \tag{16}$$

where $i \in [X^2\Sigma^+, A^2\Pi, B^2\Sigma^+]$, $j \in [A^{so}, V^{so}_{AB}, V^{so}_{AX}, L_{AB}, L_{AX}]$ and $\mathrm{a_p}$ - non-linear fitting parameters of the global deperturbation model above (2.1).

The experimental rovibronic termvalues E^{exp}_j of the $X \sim A \sim B$ complex and their uncertainties σ^{exp}_j were borrowed from Ref. [5]. The fitted zero-point-energy $\mathrm{ZPE_{fit}}$ included in Eq.(15) is responsible for the uniformed systematic shift of an origin of all experimental term values involved. The χ^2_{ab} term (16) was added to the conventional sum χ^2_{exp} (15) in order to provide the physically correct behavior of the fitting electronic parameters of the deperturbation model outside the current experimental region. The *ab initio* potentials, U^{ab}_i, and the corresponding electronic matrix elements $f^{ab}_j \in [A^{so}, V^{so}_{AB}, V^{so}_{AX}, L_{AB}, L_{AX}]$ as a discrete functions of interatomic distance $r_k \in [0.85, 4.0]$ Å, were borrowed from Ref. [16]. Their uncertainties, $\sigma^{ab}(r_k)$, were determined as the residual of the relevant point-wise functions evaluated at the r_k points using two $aug-cc-pCVnZ$ atomic basis sets with cardinal numbers $n = 5$ and 6, respectively.

The minimum of the total $\chi^2_{total}(\mathrm{a_p})$ functional was searched using the robust Levenberg-Marquardt algorithm realized in the MINPACK program suit [24]. The required Jacobian matrix was calculated numerically at each iteration by the central finite-difference (FF) schema. Overall number of fitting parameters $\mathrm{a_p}$ were reached up to 65 depending of the deperturbation model

used. The non-adiabatic E_j^{CC} eigenvalues in Eq.(15) were obtained using the iterative numerical solution of the 4×4 CC equations (1) defined on the interval $r \in [0.85; 2.85]$ Å. The corresponding band matrix was constructed by the five-points central FF approximation of the kinetic energy term in radial Hamiltonian with the fixed number of grid points $M = 1200$. The adaptive analytical mapping procedure [25] based on the reduced variable (11) with the parameters of $p = 5$ and $r_{\rm ref} = 1.2$ Å and an analytical extrapolation to zero step of the integration ($M \to \infty$) were both implemented to minimize a truncation error in the resulting eigenvalues up to 0.001-0.005 cm^{-1}.

3. Results and Discussion

3.1. Rovibronic term values of the $^{12}C^{14}N$ isotopomer

Three data sets of experimental rovibronic terms of the most abundant ^{12}C^{14}N isotopomer (see Table 1) were successively involved in the global RCC deperturbation analysis, which was realized due to the non-linear least squares fitting (NLSF) procedure described above. The first squeeze set (`set-I`) was restricted by the low vibrational quantum numbers $v_X \in [0, 12]$, $v_A \in [0, 16]$ and $v_B \in [0, 10]$ of the states treated. The intermediate set (`set-II`) consisted of the vibrational terms $v_X \in [0, 18]$, $v_A \in [0, 22]$ and $v_B \in [0, 12]$. The largest set (`set-III`) included all experimental term values available for $v_X \leq 18$, $v_A \leq 22$ and $v_B \leq 19$ levels from the refined experimental MARVEL data [7]. The maximal rotational quantum numbers J^{max} were not limited in all sets above. N_{total}^{exp} is a total number the experimental term values belonging to each set while N_{fit}^{exp} is a particular number of the experimental term values actually included in the fitting procedure (15). $N_{total}^{exp} > N_{fit}^{exp}$ since the term values with the experimental uncertainty $\sigma_j^{exp} > 0.07$ cm^{-1} were excluded from the fit.

A comparison of the root-mean-square (RMS) deviations derived by using of the three experimental data sets are given on Table 1. The rotationally averaged residual of the present (RCC), traditional EHA (Mollist) and Duo rovibronic energy levels from the their experimental MARVEL counterparts corresponding to vibrational levels of the $X^2\Sigma^+$, $A^2\Pi$ and $B^2\Sigma^+$ states are presented on Tables 2, 3 and 4, respectively. Figures 2, 3 and 4 visually compare the rovibronic terms predicted for the $X \sim A \sim B$ complex in the framework of the traditional EHA (Mollist) and the present RCC model against 5608 Marvel empirical energy levels.

It is clearly seen that the overall RMSD of 0.015 cm^{-1} obtained for the `set-I` is comparable with accuracy of the band-by-band EH approach and in order of magnitude better then the global Duo method (see, for instance, Fig.3 of Ref.). The vast majority of the RCC energy levels are closer to the empirical energy levels than those generated using the perturbative EHA. The most significant improvement in the RCC model, comparing with the EHA, is observed for lowest locally perturbed $v_X = 11$, $v_A = 3 - 8$ and $v_B = 0, 3, 5$ vibrational levels of the $X \sim A \sim B$ complex. Simultaneously, the present RCC model allows one to reproduce the entire Λ-doubling effect in the complex with a pseudo-spectral accuracy. As expected the most problematic in all deperturbation models under consideration are the highest vibrational levels, especially it concerns the $B^2\Sigma^+$ state. It seems to be attributed to additional interaction with the "dark" quartet and sixtet states manifold. Note that the fitted correction $\delta_{\rm ZPE}$ to the total zero-point-energy ZPE$_{\rm fit}$ in Eq.(15) is found to be stably small but not negligible for any input data sets.

3.2. Interatomic EMO potentials

The resulting parameters of empirical EMO potentials derived for the $X^2\Sigma^+$, $A^2\Pi$ and $B^2\Sigma^+$ states of CN based on the `set-I` of experimental term values are presented in Table 6. The

Table 1: The root-mean-square deviations (RMSD) obtained for three experimental data sets (`set I-III`) of the refined MARVEL [7] rovibronic term values of the $X^2\Sigma^+ \sim A^2\Pi \sim B^2\Sigma^+$ complex of the major $^{12}C^{14}N$ isotopomer. ZPE_{fit}=1031.060+δ_{ZPE} is the empirical zero-point-energy which corresponds to the lowest rovibronic level ($v_X = 0$, $J = 1/2$, e-parity) of the ground $X^2\Sigma^+$ state. The δ_{ZPE}-value is treated here as a small correction to be adjusted during the fit. The ZPE_{CC} is the CC energy evaluated by means of the corresponding set of the deperturbed molecular parameters. All energies are given in cm^{-1}.

Set	v_X^{max}	v_A^{max}	v_B^{max}	$N^{exp}_{total/fit}$	RMSD	δ_{ZPE}	ZPE_{fit}	$ZPE_{fit} - ZPE_{CC}$
I	12	16	10	5620/5608	0.015	0.075	1031.135	0.012
II	18	22	12	6483/6311	0.030	0.086	1031.146	-0.003
III	18	22	19	6838/6566	0.050	0.090	1031.150	0.025

Table 2: The rotationally averaged deviation of the present, Mollist and Duo (PW/Mollist/Duo) rovibronic energy levels from the their Marvel counterparts are derived for the ground $X^2\Sigma^+$ state. $\Delta E^{max} = \max|E_J^{Calc} - E_J^{Marvel}|$. All deviations are in cm^{-1}.

v_X	J_X^{max}	Mean	RMSD	ΔE^{max}
0	97.5	-0.000/-0.01/-0.01	0.007/0.02/0.05	0.02/0.05/0.19
1	99.5	-0.000/-0.01/0.02	0.008/0.02/0.05	0.03/0.05/0.19
2	97.5	0.000/-0.01/0.01	0.009/0.02/0.06	0.04/0.03/0.21
3	81.5	0.001/-0.01/0.00	0.008/0.02/0.03	0.04/0.03/0.10
4	72.5	-0.000/-0.01/-0.02	0.007/0.02/0.04	0.05/0.05/0.14
5	60.5	-0.001/-0.01/-0.04	0.004/0.01/0.04	0.015/0.03/0.07
6	48.5	-0.000/-0.00/-0.04	0.004/0.01/0.04	0.016/0.05/0.05
7	36.5	-0.001/-0.01/0.03	0.004/0.01/0.03	0.01/0.03/0.05
8	34.5	-0.001/-0.01/0.01	0.004/0.01/0.03	0.015/0.03/0.06
9	30.5	0.001/-0.01/0.04	0.003/0.01/0.05	0.01/0.02/0.12
10	27.5	-0.003/-0.01/0.07	0.015/0.02/0.07	0.05/0.07/0.17
11	36.5	-0.006/0.59/0.10	0.14/1.89/0.19	0.36/5.93/0.57
12	19.5	-0.000/-0.00/0.05	0.008/0.02/0.06	0.02/0.05/0.11
13	23.5	0.02/-0.00/-0.04	0.15/0.10/0.12	0.72/0.52/0.53
14	37.5	0.19/0.03/-0.38	0.74/0.17/0.63	3.39/0.65/2.83
15	22.5	0.37/0.10/0.16	0.22/0.15/0.23	1.02/0.54/0.68
16	29.5	-0.20/ - /-0.51	0.30/ - /0.58	0.51/ - /0.99
17	32.5	0.85/ - /0.55	1.16/ - /1.22	3.39/ - /3.01
18	23.5	0.08/ - /-0.08	0.23/ - /0.22	0.77/ - /0.51

Table 3: The rotationally averaged deviation of the present, Mollist and Duo (PW/Mollist/Duo) rovibronic energy levels from the their Marvel counterparts are derived for the $A^2\Pi$ state. $\Delta E^{max} = \max|E_J^{Calc} - E_J^{Marvel}|$. All deviations are in cm^{-1}.

v_A	J_A^{max}	Mean	RMSD	ΔE^{max}
0	98.5	0.001/-0.01/-0.02	0.007/0.02/0.20	0.02/0.06/0.78
1	98.5	-0.001/-0.01/0.06	0.006/0.01/0.18	0.03/0.03/0.61
2	80.5	0.001/-0.01/0.07	0.012/0.01/0.14	0.19/0.04/0.36
3	99.5	-0.001/-0.02/0.00	0.006/0.11/0.15	0.03/1.14/0.47
4	97.5	0.001/-0.00/-0.05	0.008/0.08/0.16	0.06/0.98/0.41
5	94.5	0.001/-0.04/-0.06	0.010/0.30/0.17	0.05/3.14/0.45
6	82.5	0.001/-0.08/-0.06	0.010/0.41/0.17	0.04/3.83/0.47
7	37.5	0.001/-0.30/-0.05	0.066/1.15/0.11	0.17/4.82/0.27
8	41.5	-0.001/0.27/0.02	0.013/1.05/0.09	0.15/7.61/0.29
9	65.5	-0.001/-0.03/0.06	0.011/0.06/0.19	0.07/0.33/0.54
10	39.5	-0.005/-0.01/0.14	0.005/0.03/0.19	0.01/0.28/0.31
11	19.5	0.002/-0.01/0.21	0.007/0.01/0.24	0.03/0.02/0.35
12	22.5	0.001/-0.00/0.22	0.008/0.01/0.25	0.03/0.03/0.37
13	21.5	0.005/-0.01/0.20	0.008/0.01/0.23	0.03/0.03/0.36
14	20.5	0.003/-0.01/0.14	0.007/0.01/0.18	0.02/0.02/0.29
15	23.5	0.004/-0.00/0.05	0.008/0.02/0.11	0.03/0.19/0.19
16	24.5	-0.007/-0.01/-0.08	0.009/0.01/0.13	0.008/0.04/0.44
17	22.5	-0.002/0.01/0.08	0.01/0.16/0.67	0.04/0.60/3.15
18	23.5	-0.001/-0.00/-0.22	0.06/0.04/0.25	0.17/0.27/0.56
19	22.5	-0.006/-0.01/-0.30	0.013/0.01/0.33	0.01/0.06/0.62
20	19.5	0.003/-0.01/-0.26	0.01/0.01/0.34	0.04/0.04/0.94
21	21.5	-0.001/-0.01/0.03	0.02/0.02/0.27	0.03/0.13/0.40
22	20.5	0.001/-0.00/0.30	0.01/0.01/0.45	0.03/0.04/0.72

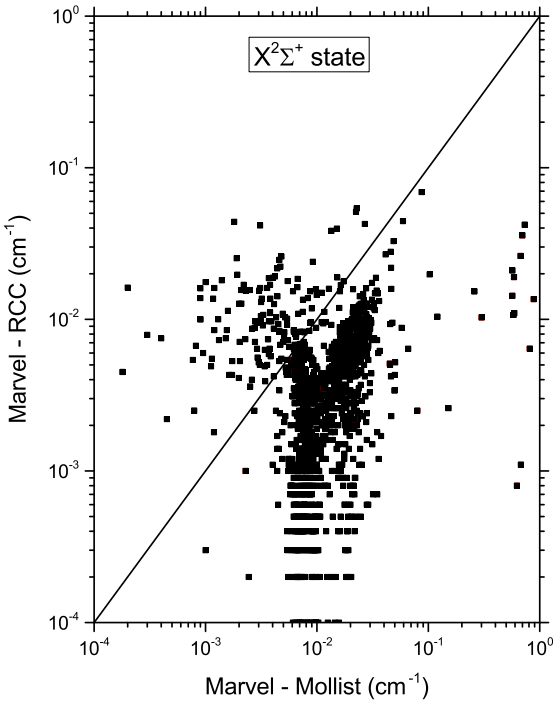

Figure 2: Comparison of the residuals with experimental term values (Marvel) corresponding to the `set-I` ($v_X \in [0, 12]$) of the ground state from traditional EHA (Mollist) and the present (RCC) calculations.

alternative EMO parameters obtained with a help of two others extended sets are given Tables 7 and 8, respectively. The corresponding EMO PECs are depicted on Fig. 1 as well.

The required initial set of EMO parameters for the isolated (deperturbed) X, A and B states were obtained during the NLSF of a merged set of the corresponding point-wise empirical (Rydberg-Klein-Rees) [17, 10] and *ab initio* potentials [16]. The electronic term $T_e(X) \equiv 0$ and dissociation energy $D_e(X)$ of the ground X-state were both fixed during the fit. The taken D_e(X)=62800.0 value (in cm^{-1}) is the *ab initio* estimate borrowed from Ref. [16]. The electronic terms of the excited A and B states were constrained as $T_e(A) = D_e(X) - D_e(A)$ and $T_e(B) = D_e(X) - D_e(B) + \Delta E$, respectively. $\Delta E = E_{^2D}(N) - E_{^4S}(N) = 19229.6$ cm^{-1} is the difference of the experimental nitrogen terms [26] (see Fig. 1). The dissociation energies of the excited states, $D_e(A)$ and $D_e(B)$, as well as the equilibrium distance, r_e, and polynomial coefficients, β_i, were treated as the adjusted fitting parameters of the EMO potential, whereas p and $r_{\rm ref}$ parameters were fixed (see Sec.2.3 for details). For each of the electronic states, dozen expansion β - coefficients appearing in Eq.(10) turned out to be sufficient. The equilibrium parameters and the lowest β_i - coefficients of EMO potentials are found to be rather stable with respect to input term values set whereas the higher β_i - coefficients expectably demonstrate more higher volatility

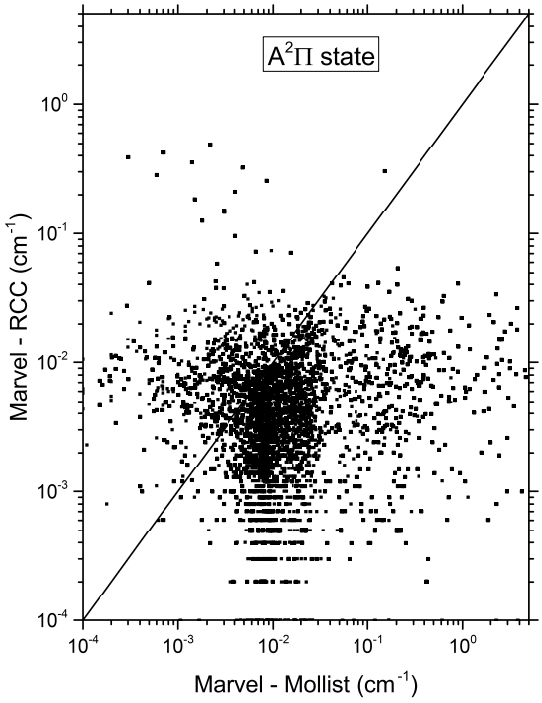

Figure 3: Comparison of the residuals with experimental term values (Marvel) corresponding to the `set-I` ($v_A \in [0, 16]$) of the $A^2\Pi$ state from traditional EHA (Mollist) and the present (RCC) calculations.

(please, compare β_i-values in Tables 6, 7 and 8).

The resulting EMO potential energy curves of all states of the $X \sim A \sim B$ complex deviate of from their empirical RKR analogs within a few tens of cm^{-1} across the experimental energy region available for each state. Outside of the experimental data region EMO PECs of the ground and first excited states also agree very well with their *ab initio* counterparts from Ref. [16]. However, the EMO potential of the $B^2\Sigma^+$ state demonstrates a noticeable deviation from the *ab initio* potential at large internuclear distances, probably due to indirect impact of the neglected perturbations.

Table 9 compares the equilibrium spectroscopic constants obtained for the present EMO PECs against previous empirical and *ab initio* data, including those exploited to generate Mollist (EHA) and EXOMOL (Duo) lists, respectively. The present RCC parameters for all three states agree the best with their EHA counterparts. The extremely small difference between the EHA and RCC spectroscopic constants (in particular, observed for equilibrium distances) are likely to be responsible for a pseudo-spectroscopic accuracy in our calculated energy levels.

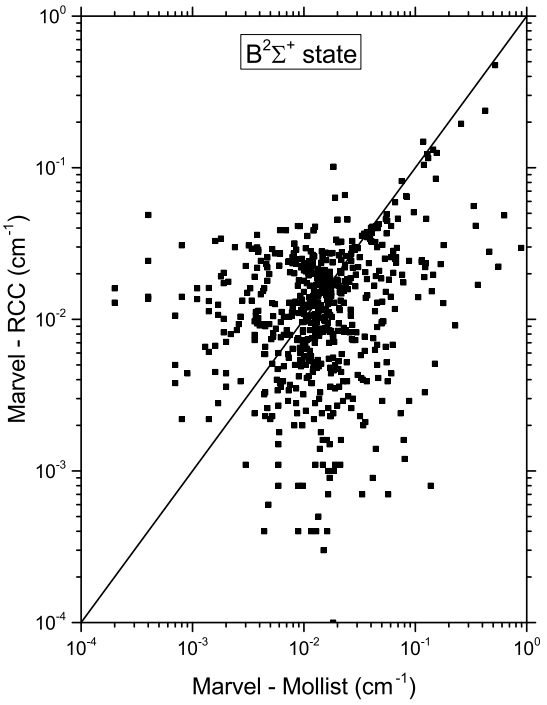

Figure 4: Comparison of the residuals with experimental term values (Marvel) corresponding to the `set-I` ($v_B \in [0, 10]$) of the $B^2\Sigma^+$ state from traditional EHA (Mollist) and the present (RCC) calculations.

3.3. Spin-orbit and L-uncoupling matrix elements

The resulting spin-orbit and L-uncoupling electronic matrix elements responsible for SO splitting of the $A^2\Pi$ state and overall non-adiabatic interactions inside of the $X \sim A \sim B$ complex are depicted on Figures 5 and 6. Open squares on both figures denote the previous empirical values [29, 30]. The currently adjusted $\alpha_0 \approx 1$ and $\alpha_1 \approx 0$ coefficients of the scaling function (13), which were used for morphing of *ab initio* SO and L-uncoupling functions [16] in according with Eq.(12), are given on Table 10.

In general, both SO and L-uncoupling matrix elements demonstrate a very weak sensitivity to particular set of input experimental energies of the complex used in the NLSF fitting. Across them L-uncoupling functions are found to be the most stable ones. The maximal deviation of the morphed L_{AX} and L_{AB} functions from their *ab initio* counterparts in entire r-range $r \in [0.7, 4.0]$ Å do not exceed 0.01 and 0.04 *a.u.*, respectively (see Fig. 6). All optimized coupled functions are remarkably close to their empirical counterparts previously extracted from a locally perturbed levels of the complex in the framework of traditional band-by-band effective Hamiltonian approach. The most significant residual (reaching up 1-2 cm^{-1} at small and intermediate distances) is observed for the diagonal spin-orbit splitting A^{so} function (see Fig. 5).

Table 4: The rotationally averaged deviation of the present, Mollist and Duo (PW/Mollist/Duo) rovibronic energy levels from the their Marvel counterparts are derived for the $B^2\Sigma^+$ state. $\Delta E^{max} = \max|E_J^{Calc} - E_J^{Marvel}|$. All deviations are in cm^{-1}.

v_B	J_B^{max}	Mean	RMSD	ΔE^{max}
0	63.5	0.003/-0.01/ 0.02	0.007/0.03/0.09	0.13/0.16/0.37
1	41.5	-0.016/-0.02/0.02	0.019/0.02/0.05	0.03/0.05/0.07
2	23.5	0.017/-0.02/1.20	0.014/0.03/1.28	0.04/0.07/1.72
3	22.5	0.015/0.11/-0.10	0.016/0.88/0.57	0.07/6.01/1.31
4	23.5	-0.009/-0.01/-1.16	0.010/0.02/1.27	0.01/0.05/2.23
5	24.5	-0.018/0.02/-1.91	0.024/0.37/2.09	0.065/1.71/3.72
6	25.5	-0.002/-0.01/-1.19	0.008/0.01/1.28	0.017/0.02/2.12
7	19.5	0.025/-0.05/0.22	0.082/0.12/0.35	0.47/0.52/1.60
8	26.5	0.011/-0.01/0.72	0.008/0.01/0.80	0.03/0.04/1.16
9	26.5	-0.023/-0.03/1.55	0.05/0.07/1.56	0.12/0.42/2.35
10	24.5	0.009/-0.00/0.84	0.013/0.09/1.03	0.06/0.33/2.03
11	36.5	-0.025/-0.05/0.51	0.19/0.13/1.23	0.29/0.63/6.43
12	15.5	-0.012/-0.04/-0.89	0.026/0.11/1.01	0.017/0.48/1.28
13	21.5	-0.015/-0.00/-2.00	0.03/0.02/2.00	0.06/0.05/2.12
14	37.5	-0.05/-0.08/-0.74	1.01/0.69/4.35	5.13/3.16/30.1
15	19.5	0.59/0.08/-0.20	0.06/0.13/0.31	0.73/0.500.62
16	37.5	-0.97/ - /2.66	2.45/ - /6.45	6.45/ - /38.0
17	30.5	-0.05/ - /3.34	1.59/ - /3.61	4.95/ - /7.18
18	33.5	0.58/ - /5.20	2.87/ - /7.30	13.9/ - /30.3
19	23.5	0.10/ - /0.22	0.12/ - /0.32	0.33/ - /0.94

3.4. Λ-doubling parameters

The fitting α_0 and α_1 parameters of the pure empirical second order Λ-doubling parameters derived for the $A^2\Pi$ state are presented on the Table 11. The adjusted parameters of the scaling $S(r)$ function used for morphing of the *ab initio* γ_X function in Eq.(14) for the ground $X^2\Sigma^+$-state are given on the Table 12. It should be remind that the q_X parameter of the X-state was fixed on its *ab initio* counterpart from [16] while the relevant γ_B and q_B parameters of the excited $B^2\Sigma^+$ state were completely neglected in the present deperturbation model (compare Eq.(2) with Eq.(5)).

All second order correction parameters demonstrate a high volatility with respect to the particular experimental term values used: sets I/II/III (see details on Table1). The most pronounced variations are observed to be $p_{A\Delta}$ and $q_{A\Delta}$ functions. Nevertheless, the present empirical α_0 values still reasonably agree their *ab initio* counterparts α_0^{ab} calculated in Ref. [16].

The derived empirical p and q functions on Table 11 are found to be less by an order of magnitude then their conventional Λ-doubling counterparts obtained for the lowest $v_A \in [0, 6]$ vibrational levels of the $A^2\Pi$ state in the framework of the Effective Hamiltonian approach [10]. At the same time, the present γ_X function (14) is only 2-2.5 times less then the corresponding experimental γ_X-values derived for the lowest $v_X \in [0, 10]$ levels of the ground state [31].

3.5. Line positions of the minor $^{12}C^{15}N$ and $^{13}C^{14,15}N$ isotopomers

It should be emphasized that all parameters of the modeling Hamiltonian in Sec.2.1 depends on the reduced molecular mass μ in an explicit form. Furthermore, both adjusted and fixed

Table 5: Extract from the output listing file corresponding to the experimental term values `set-I` and the mutually perturbed $A^2\Pi_{1/2}(v_A = 7) \sim X^2\Sigma^+(v_X = 11)$ f-parity rovibronic levels of $^{12}C^{14}N$. Full tables are available in the Supplementary materials 5. All energies in cm^{-1} while the fractional partition P_i in %. $\Delta = E^{exp} - E^{CC}$

$J + 1/2$	E^{exp}	σ^{exp}	E^{CC}	Δ	$P_{A_{1/2}}$	$P_{A_{3/2}}$	P_X	P_B
1	22152.9498	0.0312	22152.9393	0.0105	99.7	0.0	0.3	0.0
2	22157.8303	0.0211	22157.8364	-0.0060	99.4	0.2	0.3	0.0
3	22165.9932	0.0150	22165.9925	0.0007	99.0	0.6	0.4	0.0
4	22177.4047	0.0068	22177.4051	-0.0004	98.5	1.2	0.4	0.0
5	22192.0705	0.0076	22192.0707	-0.0002	97.8	1.8	0.4	0.0
6	22209.9764	0.0139	22209.9852	-0.0089	97.0	2.6	0.4	0.0
7	22231.1440	0.0085	22231.1439	0.0001	96.1	3.5	0.4	0.0
8	22255.5414	0.0071	22255.5415	-0.0001	95.2	4.4	0.4	0.0
9	22283.1736	0.0080	22283.1725	0.0011	94.2	5.4	0.4	0.0
10	22314.0344	0.0052	22314.0313	0.0032	93.1	6.5	0.4	0.0
11	22348.1140	0.0083	22348.1119	0.0021	92.0	7.5	0.5	0.0
12	22385.4127	0.0048	22385.4086	0.0041	90.9	8.6	0.5	0.0
13	22425.9194	0.0048	22425.9157	0.0037	89.8	9.7	0.5	0.0
14	22469.6336	0.0049	22469.6275	0.0061	88.7	10.7	0.6	0.0
15	22516.5425	0.0049	22516.5386	0.0039	87.6	11.8	0.6	0.0
16	22566.6497	0.0049	22566.6438	0.0059	86.5	12.8	0.7	0.0
17	22619.9439	0.0049	22619.9383	0.0056	85.4	13.8	0.8	0.0
18	22676.4232	0.0049	22676.4176	0.0057	84.4	14.8	0.9	0.0
19	22736.0840	0.0049	22736.0777	0.0063	83.3	15.7	1.0	0.0
20	22798.9222	0.0049	22798.9157	0.0065	82.2	16.6	1.2	0.0
21	22864.9369	0.0054	22864.9302	0.0068	81.1	17.4	1.5	0.0
22	22934.1273	0.0054	22934.1221	0.0052	80.0	18.1	1.9	0.0
23	23006.5035	0.0054	23006.4980	0.0055	78.6	18.8	2.6	0.0
24	23082.0812	0.0054	23082.0761	0.0051	76.9	19.2	3.9	0.0
25	23160.9100	0.0060	23160.9053	0.0048	74.3	19.2	6.5	0.0
26	23243.1358	0.0060	23243.1307	0.0051	68.6	18.2	13.2	0.0
27	23329.2507	0.0060	23329.2415	0.0092	53.1	14.1	32.8	0.0
28	23411.4969	0.0069	23411.4946	0.0024	51.4	17.4	31.2	0.0
29	23503.9219	0.0060	23503.9213	0.0007	66.6	22.2	11.2	0.0
30	23598.6782	0.0069	23598.6711	0.0071	71.1	24.1	4.8	0.0
31	23696.2519	0.0085	23696.2595	-0.0076	72.4	25.1	2.5	0.0
32	23796.8497	0.0120	23796.8412	0.0085	72.7	25.8	1.5	0.0

Table 6: The resulting fitted parameters of EMO potential energy curves (defined by the relations (9)-(11)) for the $X^2\Sigma^+$, $A^2\Pi$ and $B^2\Sigma^+$ states of CN obtained using the `set-I` of experimental term values (see Table 1). T_e is the electronic term, D_e is the dissociation energy are given in cm^{-1}, while the equilibrium bond lengths, r_e, and the reference distance, r_{ref}, are given in Å. The polynomial expansion coefficients, β_i are dimensionless. $p = 3$ and $N = 11$ for all states. The symbol ‡ means the fixed parameters.

	$X^2\Sigma^+$	$A^2\Pi$	$B^2\Sigma^+$
T_e	‡0.0	9244.990	25753.268
D_e	‡62800.0	53555.010	56276.424
r_e	1.1717581432	1.2328109635	1.1512467113
$^\ddagger r_{ref}$	1.2	1.4	1.2
β_0	2.5661841875	2.4711516802	2.8428969376
β_1	0.3131893375	0.3072809872	0.3192612426
β_2	0.4000377522	0.4215078990	-0.4943078572
β_3	0.4082731310	0.4759502604	-2.2708079658
β_4	0.6117640276	0.5758112596	-7.2050711568
β_5	0.7904831415	0.5231053751	-23.4328121497
β_6	0.0439995268	0.5343730971	0.0895487135
β_7	0.9040290061	0.0013014662	221.1275319867
β_8	8.3341106959	-1.9048447097	218.7315527295
β_9	-0.0059200320	-2.4795165771	-720.6420260873
β_{10}	-16.7936431296	-0.0024682491	-549.9897275429
β_{11}	13.5541978986	0.0001605346	994.9287021111

Table 7: The resulting fitted parameters of EMO potential energy curves (defined by the relations (9)-(11)) for the $X^2\Sigma^+$, $A^2\Pi$ and $B^2\Sigma^+$ states of CN obtained using the `set-II` of experimental term values (see Table 1).

	$X^2\Sigma^+$	$A^2\Pi$	$B^2\Sigma^+$
T_e	‡0.0	9244.977	25753.303
D_e	‡62800.0	53554.997	56276.389
r_e	1.1717566069	1.2325912020	1.1512540586
$^\ddagger r_{ref}$	1.2	1.4	1.2
β_0	2.5662285705	2.4712196994	2.8430062880
β_1	0.3108303801	0.3074053839	0.3214099993
β_2	0.4021595795	0.4210878161	-0.5089112484
β_3	0.5272110175	0.4779785895	-2.3070618533
β_4	0.4821817698	0.5921043055	-6.9391183259
β_5	-0.5540577244	0.5023281633	-23.7889536523
β_6	-0.3051241007	0.4081872717	0.0103354345
β_7	-1.1730128576	0.0001074838	229.1497599253
β_8	53.7322037048	-1.8420243127	198.0057727766
β_9	0.1373774983	-2.7077295959	-745.5697268135
β_{10}	-275.2562159084	0.0000256700	-466.7768528456
β_{11}	282.1395321217	-0.0027726883	953.8342605062

Table 8: The resulting fitted parameters of EMO potential energy curves (defined by the relations (9)-(11)) for the $X^2\Sigma^+$, $A^2\Pi$ and $B^2\Sigma^+$ states of CN obtained using the `set-III` of experimental term values (see Table 1).

	$X^2\Sigma^+$	$A^2\Pi$	$B^2\Sigma^+$
T_e	‡0.0	9245.005	25753.606
D_e	‡62800.0	53554.982	56276.752
r_e	1.1717555034	1.2327700637	1.1512176850
‡r_{ref}	1.2	1.4	1.2
β_0	2.5661027061	2.4711811388	2.8422538104
β_1	0.3145503689	0.3072409694	0.2923449444
β_2	0.4039728728	0.4196612220	-0.3211634660
β_3	0.1891128708	0.4851495934	-1.2383046312
β_4	1.0083521985	0.6303722209	-13.2275002738
β_5	8.7213169677	0.4290056433	-38.0908930460
β_6	-21.4577463705	0.0001739374	77.0282917319
β_7	-92.5389676528	0.0002708831	309.1082236918
β_8	326.7620724001	-0.3415171811	-169.1125209557
β_9	199.1686195517	-1.0576679839	-935.3697396234
β_{10}	-1405.8239120908	0.0006740631	30.8321202452
β_{11}	1123.1322205501	-0.0058020396	1193.0110454954

Table 9: A comparison of the electronic term, T_e, the dissociation energy, D_e, and the equilibrium distance, r_e, obtained for the $X^2\Sigma^+$, $A^2\Pi$ and $B^2\Sigma^+$ states of $^{12}C^{14}N$ radical by means of alternative deperturbation analysis and direct *ab initio* calculation. RCC - reduced coupled-channel deperturbation analysis performed in the present work; EHA - conventional effective Hamiltonian approach (EHA) [11]; Duo - coupled-channel deperturbation analysis [15] in the framework of Duo paradigm [14]; Expt. - experimental measurement [27]; *ab* - first principle electronic structure calculation [28]. The electronic term of the ground state was fixed to be zero at all methods.

	$X^2\Sigma^+$	$A^2\Pi$	$B^2\Sigma^+$	Source
T_e/cm^{-1}	0.0	9244.991(15)	25753.4(3)	RCC
	0.0	9243.296(5)	25752.59(1)	EHA
	0.0	9246.87	25755.6	Duo
	0.0	9109.95	25776.4	*ab*
D_e/cm^{-1}	62800.0[ab]	53555.00(2)	56276.5(3)	RCC
	62588.6			Expt.
	63619.4	63619.4	57087.5	Duo
	63077.4	53968.2	56659.5	*ab*
$r_e/Å$	1.171757(2)	1.23272(9)	1.15123(2)	RCC
	1.1718063(9)	1.2330449(9)	1.15133(12)	EHA
	1.17272	1.23135	1.14979	Duo
	1.1714	1.2324	1.151	*ab*

Table 10: The dimensionless $\alpha_{0,1}$ parameters of the linear $S(r)$ function (13) used for morphing of *ab initio* spin-orbit and L-uncoupling electronic matrix elements [16] in according to Eq.(12). The f_∞-values were fixed on their asymptotic atomic counterparts.

	A^{so}/cm^{-1}	$V^{so}_{AX}/\mathrm{cm}^{-1}$	$V^{so}_{AB}/\mathrm{cm}^{-1}$
α_0	1.0452/1.0454/1.0453	1.0326/1.0329/1.0270	1.0045/1.0075/0.9886
α_1	-0.0590/-0.0709/-0.0613	-0.0005/0.0003/0.0210	0.0002/-0.0000/-0.0002
f_∞	-4.66	+6.59	0.0
	$L_{AX}/a.u.$	$L_{AB}/a.u.$	
α_0	1.0066/1.0068/1.0064	0.9712/0.9810/0.9858	
α_1	0.0000/0.0004/0.00005	-0.0184/-0.0073/0.0001	
f_∞	$-\sqrt{2}$	0.0	

Table 11: The coefficients of the $S(r)$ function (13) is used to represent the empirical p_A, $p_{A\Delta}$ (dimensionless) and q_A, $q_{A\Delta}$ (in $1/\mathrm{cm}^{-1}$) functions corresponding to the second-order contribution of the remote doublet states manifold to the Λ-doubling parameters of the $A^2\Pi$ state. The resulting parameters were obtained during the NLSF of the three (I/II/III) experimental term value sets. The α^{ab}_0 values were estimated from the corresponding *ab initio* point-wise functions taken at the equilibrium point $r_e(A)$ [16].

	$p_A \times 10^{-4}$	$p_{A\Delta} \times 10^{-4}$	$q_A \times 10^{-5}$	$q_{A\Delta} \times 10^{-5}$
α^{ab}_0	-5.4	-0.81	-2.2	-5.7
α_0	-4.23/-4.60/-4.20	-4.8/-12.5/-0.77	-2.32/-2.20/-2.16	-16.0/-36.7/-3.6
α_1	0.185/0.024/-0.102	248.0/300.9/255.8	-17.2/-19.7/-22.5	-83.5/-126.0/-57.0

Table 12: The dimensionless α_0 and α_1 parameters of the $S(r)$ function (13) used in Eq.(14) for scaling of *ab initio* $\gamma_X(r)$ function form [16] for the ground $X^2\Sigma^+$ state. The coefficients were obtained during the NLSF of the three I/II/III experimental termvalue sets.

α^{ab}_0	1.00
α_0	1.32/0.94/1.14
α_1	-2.97/19.9/6.59

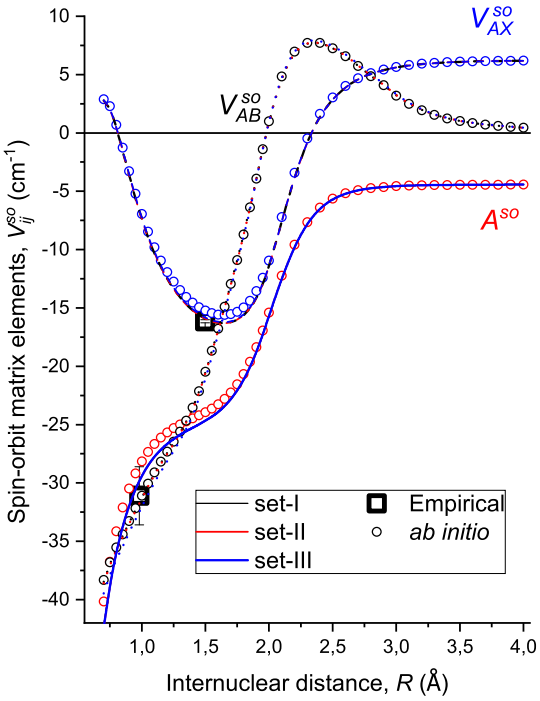

Figure 5: Comparison of the morphed spin-orbit electronic matrix elements $A^{so}(r)$, $V^{so}_{AX}(r)$ and $V^{so}_{AB}(r)$ obtained in present work by the RCC fitting of the three experimental data sets (`set I-III`) of the MARVEL term values [7]. *Ab initio* data are borrowed from Ref. [16], empirical point from Refs. [29, 30]

electronic parameters of the present global CC deperturbation model are supposed to be mass-invariant functions of internuclear distance. It is not formally true since the L-uncoupling matrix elements theoretically depend on an origin of a center mass of molecule [8]. However, this possible μ-dependance is assumed too weak for observation.

To validate mass-invariant properties of the resulting deperturbation parameters, the EMO interatomic potentials and off-diagonal coupling parameters, adjusted above using solely the $^{12}C^{14}N$ isotopomer data, were exploited for a line list prediction of rotational, vibrational and rovibronic transitions which are also observed for minor $^{13}C^{14}N$ and $^{12,13}C^{15}N$ isotopomers. It has been done just by a substitution for the proper reduced mass in Eq.(1).

For the lowest $1.5-0.5$ and $2.5-1.5$ pure rotational (neglecting hyperfine structure) transitions corresponding to $v_X \in [0,9]$ vibrational levels of both e/f components of the ground $X^2\Sigma^+$ state of $^{13}C^{14}N$ isotopomer the predicted R-line positions have coincided with their MW spectroscopic counterparts better than 10^{-4} cm^{-1}. Factually that is the same accuracy as one of the effective Hamiltonian approach. For rotational-vibrational transitions corresponding to the fundamental $1-0$ band the theoretical P/R line positions ($J \in [4,27]$) represent their experimental IR coun-

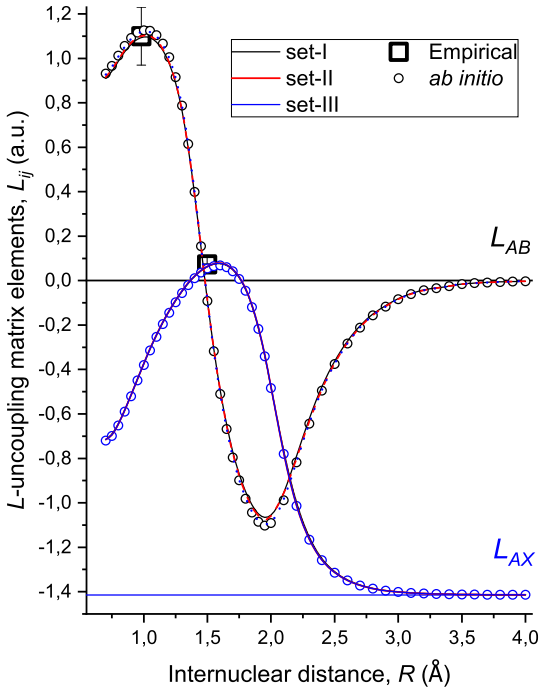

Figure 6: Comparison of the morphed L-uncoupling electronic matrix elements $L_{AX}(r)$ and $L_{AB}(r)$ obtained by the present RCC fitting of the three sets (`set I-III`) of the MARVEL experimental term values [7]. The corresponding *ab initio* points are taken from Ref. [16], empirical point from Refs. [29, 30]

terparts with r.m.s. deviation is about of 0.004 cm^{-1} and a systematic shift (Exp. - Calc.) of +0.001, +0.007 and +0.01 cm^{-1} for ^{12}C^{15}N, ^{13}C^{15}N and ^{13}C^{14}N isotopomers, respectively.

In the case of $A-X$ and $B-X$ electronic transitions a systematic divergence of the theoretical rovibronic line positions from the corresponding experimental data becomes much more pronounced (see, for example, Table 13). However, this mainly concern the so-called electronic and vibrational isotopic shifts whereas the J-dependance of the observed deviations are normally very weak. It means that the rotational molecular constants derived in the framework of the present CC deperturbation analysis, including Λ-doubling functions, are really mass-independent. The isotopic shift of the $A-X$ bands of both isotopologues weakly depends on vibrational excitation while the analogue $B-X$ bands isotopic shifts increase as v_B-values increases. The main part of electronic isotopic shifts observed in both $A-X$ and $B-X$ systems seems to be attributed to a mass-dependant adiabatic correction formally ignored in the present EMO potentials. The pronounced v-dependance of the $B-X$ shift can be raised from non-adiabatic coupling taking place between $^2\Sigma^+$ states manifold. The recent *ab initio* electronic structure calculation [16] claimed indeed that the radial coupling matrix element between $B^2\Sigma^+$ and $X^2\Sigma^+$ states is large enough

Table 13: Systematic shifts and r.m.s. deviations (in cm^{-1}) extracted from the residual of experimental line positions from their theoretical counterparts belonging to of several bands of $A-X$ and $B-X$ systems of minor CN isotopologues. The line positions were predicted in the framework of the present RCC deperturbation model using the `set-I` of the mass-invariant molecular parameters.

Band	J^{max}	Mean	RMSD	J^{max}	Mean	RMSD
		$^{13}C^{14}N$			$^{12}C^{15}N$	
$A-X$ system						
0-1	82.5	-0.209	0.006	48.5	-0.135	0.004
1-2	50.5	-0.221	0.006	48.5	-0.146	0.004
2-4	52.5	-0.230	0.006	43.5	-0.144	0.005
3-1	64.5	-0.218	0.007	34.5	-0.149	0.008
4-2	52.5	-0.221	0.006	46.5	-0.154	0.010
$B-X$ system						
0-0	39.5	-0.055	0.014	46.5	-0.03	0.02
1-2	34.5	-0.106	0.016	30.5	-0.05	0.02
2-3	30.5	-0.100	0.035			
3-4	22.5	-0.114	0.008			
4-4	23.5	-0.155	0.012			
5-4	23.5	-0.185	0.012			

in entire range of internuclear distance. Therefore, the non-adiabatic coupling between $B^2\Sigma^+$ and $X^2\Sigma^+$ states was explicitly concerned in the present CC deperturbation model by introducing the non-vanishing off-diagonal electronic matrix element $V^{el}_{XB}(r)$ which is responsible for the electrostatic interaction of the X and B diabatic states. However, the resulting empirical $V^{el}_{XB}(r)$ functions were found to be unexpected small for all input sets.

4. Concluding remarks

A direct global deperturbation analysis of the 5600-6570 experimental rovibronic term values belonging to the $X^2\Sigma^+$, $A^2\Pi$ and $B^2\Sigma^+$ states of the $^{12}C^{14}N$ isotopomer has been performed in the framework of the reduced 4×4 coupled-channel (RCC) deperturbation model based on analytical (EMO) potential energy curves (PECs) as well as *ab initio* spin-orbit and L-uncoupling electronic matrix elements between all states of the $X\sim A\sim B$ complex. The regular second order intramolecular interaction of the complex with the excited states manifold insets about 30-40% into the experimental γ-splitting parameter of the ground X-state and contributes almost nothing into its counterpart for the excited B-state. The explicit accounting of the residual perturbations of the complex by excited states significantly has improved accuracy of the representation of the A-state as well. The optimized EMO interatomic potentials, electronic coupling functions and Λ-doubling parameters describe a vast majority of the empirical term values of both locally and regularly perturbed levels of the $X\sim A\sim B$ complex with r.m.s. deviation of about 0.015-0.05 cm^{-1}, which becomes comparable or even better than with the accuracy achieved in the framework of the traditional effective Hamiltonian approach. The resulting mass-invariant RCC deperturbation parameters generate rotational and rovibrational spectra lines of minor CN isotopomers with a pseudo-spectral accuracy (without a hyperfine structure). The rovibronic line positions predicted for both $A-X$ and $B-X$ electronic transitions of $^{12}C^{15}N$ and $^{13}C^{14,15}N$ isotopomers demonstrate a small systematic (electronic) shift which very weak depends on vibrational and rotational quantum numbers of transitions. We believe that the robust RCC deperturb-

bation model could significantly refine and extend a rovibronic line-list for all CN isotopomers in a wide region of vibrational and rotational quantum numbers inevitably excited under high (probably even non-equilibrium) temperature conditions.

Acknowledgements

The work was supported by the Russian Science Foundation (RSF) (grant No.22-23-00272).

5. Supplementary Materials

Files **CN-ABX-setI.txt**, **CN-ABX-setII.txt** and **CN-ABX-setIII.txt**. Output listing files of the fitting deperturbation parameters and residuals corresponding to usage of set-I, set-II and set-III of the MARVEL experimental term values, respectively.

6. Declaration of Competing Interest

The authors declare that they have no known competing financial interests or personal relationships that could have appeared to influence the work reported in this paper.

7. CRediT authorship contribution statement

Vera A. Terashkevich: Investigation, Formal analysis, Methodology, Validation. Elena A. Pazyuk: Conceptualization, Methodology, Validation, Visualization, Writing - review - editing. Andrey V.Stolyarov: Conceptualization, Project administration, Writing - review and editing, Writing original draft. Sergey N. Yurchenko: Conceptualization, Writing - review and editing, Writing - original draft.

References

[1] A. McKellar, Evidence for the Molecular Origin of Some Hitherto Unidentified Interstellar Lines, Publications of the Astronomical Society of the Pacific 52 (307) (1940) 187. doi:10.1086/125159.

[2] S. Leach, Why COBE and CN spectroscopy cosmic background radiation temperature measurements differ, and a remedy, Monthly Notices of the Royal Astronomical Society 421 (2) (2012) 1325–1330. doi:10.1111/j.1365-2966.2011.20390.x.

[3] A. M. Ritchey, S. R. Federman, D. L. Lambert, Interstellar CN AND CH^+ in diffuse molecular clouds:$^{12}C/^{13}C$ ratios and CN excitation, The Astrophysical Journal 728 (1) (2011) 36. doi:10.1088/0004-637x/728/1/36.

[4] N. Fray, Y. Bénilan, H. Cottin, M.-C. Gazeau, J. Crovisier, The origin of the CN radical in comets: A review from observations and models, Planetary and Space Science 53 (12) (2005) 1243–1262. doi:https://doi.org/10.1016/j.pss.2005.06.005.

[5] A.-M. Syme, A. Mousley, M. Cunningham, L. K. McKemmish, Diatomic rovibronic transitions as potential probes for proton-to-electron mass ratio across cosmological time, Australian Journal of Chemistry 73 (2020) 743–756. doi:10.1071/CH19448.

[6] T. Furtenbacher, A. Csaszar, J. Tennyson, Marvel: measured active rotational–vibrational energy levels, Journal of Molecular Spectroscopy 245 (2007) 115–125. doi:10.1016/j.jms.2007.07.005.

[7] A.-M. Syme, L. K. McKemmish, Experimental energy levels of $^{12}C^{14}N$ through Marvel analysis, Monthly Notices of the Royal Astronomical Society 499 (1) (2020) 25–39. doi:10.1093/mnras/staa2791.

[8] H. Lefebvre-Brion, R. W. Field, The Spectra and Dynamics of Diatomic Molecules: Revised and Enlarged Edition, Academic Press, 2004.

[9] J. M. Brown, E. Colbourn, J. Watson, F. Wayne, An effective Hamiltonian for diatomic molecules: *Ab initio* calculations of parameters of HCl^+, Journal of Molecular Spectroscopy 74 (2) (1979) 294–318. doi:https://doi.org/10.1016/0022-2852(79)90059-6.

[10] R. Ram, L. Wallace, P. Bernath, High resolution emission spectroscopy of the $A^2\Pi$–$X^2\Sigma^+$ "red" system of $^{12}C^{14}N$, Journal of Molecular Spectroscopy 263 (2010) 82–88. doi:10.1016/j.jms.2010.07.002.

[11] J. S. A. Brooke, R. S. Ram, C. M. Western, G. Li, D. W. Schwenke, P. F. Bernath, Einstein a coefficients and oscillator strengths for the $A^2\Pi$–$X^2\Sigma^+$ (Red) and $B^2\Sigma^+$–$X^2\Sigma^+$ (Violet) systems and rovibrational transitions in the $X^2\Sigma^+$ state of CN, The Astrophysical Journal Supplement Series 210 (2) (2014) 23. doi:10.1088/0067-0049/210/2/23.

[12] R. J. L. Roy, LEVEL: A computer program for solving the radial schr¨odinger equation for bound and quasibound levels.

[13] C. Western, PGOPHER: A program for simulating rotational, vibrational and electronic spectra, Journal of Quantitative Spectroscopy and Radiative Transfer 186 (2017) 221–242. doi:10.1016/j.jqsrt.2016.04.010.

[14] S. N. Yurchenko, L. Lodi, J. Tennyson, A. V. Stolyarov, Duo: A general program for calculating spectra of diatomic molecules, Computer Physics Communications 202 (2016) 262–275. doi:10.1016/j.cpc.2015.12.021.

[15] A.-M. Syme, L. K. McKemmish, Full spectroscopic model and trihybrid experimental-perturbative-variational line list for CN, Monthly Notices of the Royal Astronomical Society 505 (3) (2021) 4383–4395. doi:10.1093/mnras/stab1551.

[16] V. A. Terashkevich, E. A. Pazyuk, A. V. Stolyarov, A computational study of the non-adiabatic coupling among low-lying doublet states of the CN radical, Journal of Quantitative Spectroscopy and Radiative Transfer 276 (2021) 107916. doi:https://doi.org/10.1016/j.jqsrt.2021.107916.

[17] R. Ram, S. Davis, L. Wallace, R. Engleman, D. Appadoo, P. Bernath, Fourier transform emission spectroscopy of the $B^2\Sigma^+$–$X^2\Sigma^+$ system of CN, Journal of Molecular Spectroscopy 237 (2006) 225–231. doi:10.1016/j.jms.2006.03.016.

[18] J. H. Van Vleck, On σ-Type Doubling and Electron Spin in the Spectra of Diatomic Molecules, Phys. Rev. 33 (1929) 467–506. doi:10.1103/PhysRev.33.467.

[19] S. V. Kozlov, E. A. Pazyuk, A. V. Stolyarov, A Reduced Method of Coupled Vibrational Channels: Analysis of Regular Perturbations in the $c^3\Sigma^+_\Omega$-State of a KRb Molecule, Optics and Spectroscopy 125 (4) (2018) 464–469. doi:10.1134/S0030400X18100119.

[20] Ivanova, Milena and Stein, Alexander and Pashov, Asen and Stolyarov, Andrey and Knöeckel, Horst and Tiemann, Eberhard, The $X^2\Sigma^+$ state of LiCa studied by Fourier-transform spectroscopy, Journal of Chemical Physics 135 (17) (2011) 174303. doi:10.1063/1.3652755.

[21] Edward G. Lee and Jenning Y. Seto and Tsuyoshi Hirao and Peter F. Bernath and Robert J. Le Roy, FTIR emission spectra, molecular constants, and potential curve of ground state GeO, Journal of Molecular Spectroscopy 194 (2) (1999) 197–202. doi:https://doi.org/10.1006/jmsp.1998.7789.

[22] R. J. L. Roy, dPotFit: A computer program to fit diatomic molecule spectral data to potential energy functions, Journal of Quantitative Spectroscopy and Radiative Transfer 186 (2017) 179–196. doi:https://doi.org/10.1016/j.jqsrt.2016.06.002.

[23] A. A. Šurkus, R. J. Rakauskas, A. B. Bolotin, The generalized potential energy function for diatomic molecules, Chemical Physics Letters 105 (3) (1984) 291–294. doi:https://doi.org/10.1016/0009-2614(84)85032-0.

[24] J. More, B. Garbow, K. Hillstrom, MINPACK software for solving nonlinear equations and nonlinear least squares problems, University of Chicago, Argonne National Laboratory (1999).

[25] V. V. Meshkov, A. V. Stolyarov, R. J. Le Roy, Adaptive analytical mapping procedure for efficiently solving the radial Schrödinger equation, Phys. Rev. A 78 (2008) 052510. doi:10.1103/PhysRevA.78.052510.

[26] A. Kramida, Yu. Ralchenko, J. Reader, and NIST ASD Team, NIST Atomic Spectra Database (ver. 5.8), [Online]. Available: `https://physics.nist.gov/asd` [2021, July 29]. National Institute of Standards and Technology, Gaithersburg, MD. (2020).

[27] Y. Huang, S. A. Barts, J. B. Halpern, Heat of formation of the cyanogen radical, The Journal of Physical Chemistry 96 (1) (1992) 425–428. doi:10.1021/j100180a079.

[28] Y. Yin, D. Shi, J. Sun, Z. Zhu, Transition Dipole Moments and Transition Probabilities of the CN Radical, The Astrophysical Journal Supplement Series 235 (2) (2018) 25. doi:10.3847/1538-4365/aab26b.

[29] A. J. Kotlar, R. J. Field, J. Steinfeld, J. A. Coxon, Analysis of perturbations in the $A^2\Pi$–$X^2\Sigma^+$ "red" system of CN, Journal of Molecular Spectroscopy 80 (1980) 86–108.

[30] H. Ito, A. Kazama, K. Kuchitsu, Perturbations in the CN($B^2\Sigma^+ - X^2\Sigma^+$) tail band system Part 4. The $B^2\Sigma^+ \sim A^2\Pi$ perturbations in the v_B = 11, 14–16, 18 and 19 levels, Journal of Molecular Structure 324 (1) (1994) 29–43. doi:https://doi.org/10.1016/0022-2860(94)08223-5.

[31] V. A. Terashkevich, E. A. Pazyuk, Nature of the Fine Structure of Rotational Levels of the Ground $X^2\Sigma^+$-State of the Radical CN, Optics and Spectroscopy 129 (1) (2021) 12–17. doi:10.1134/S0030400X21010185.